bioRxiv preprint first posted online Nov. 22, 2017; doi: http://dx.doi.org/10.1101/223933. The copyright holder for this preprint (which was not peer-reviewed) is the author/funder. It is made available under a CC-BY 4.0 International license.

Aiptasia as a model to study metabolic diversity and specificity in cnidarian-dinoflagellate symbioses

Nils Rädecker[1], Jean-Baptiste Raina[2], Mathieu Pernice[2*], Gabriela Perna[1], Paul Guagliardo[3], Matt R Kilburn[3], Manuel Aranda[1] & Christian R Voolstra[1*]

[1] Red Sea Research Center, King Abdullah University of Science and Technology, Thuwal, 23955-6900, Saudi Arabia

[2] Climate Change Cluster, University of Technology Sydney, Sydney, NSW 2007, Australia

[3] Centre for Microscopy, Characterisation and Analysis, University of Western Australia, Perth, WA 6009, Australia

[*] to whom correspondence should be addressed:

Mathieu Pernice (mathieu.pernice@uts.edu.au)

Climate Change Cluster, University of Technology Sydney, Sydney, NSW 2007, Australia

Christian R Voolstra (christian.voolstra@kaust.edu.sa)

Red Sea Research Center, King Abdullah University of Science and Technology, Thuwal, 23955-6900, Saudi Arabia

Keywords

metaorganism, holobiont, carbon translocation, nitrogen uptake, *Symbiodinium*, selfish symbiont

bioRxiv preprint first posted online Nov. 22, 2017; doi: http://dx.doi.org/10.1101/223933. The copyright holder for this preprint (which was not peer-reviewed) is the author/funder. It is made available under a CC-BY 4.0 International license.

Abstract

The symbiosis between cnidarian hosts and microalgae of the genus *Symbiodinium* provides the foundation of coral reefs in oligotrophic waters. Understanding the nutrient-exchange between these partners is key to identifying the fundamental mechanisms behind this symbiosis. However, deciphering the individual role of host and algal partners in the uptake and cycling of nutrients has proven difficult, given the endosymbiotic nature of this relationship. In this study, we highlight the advantages of the emerging model system Aiptasia to investigate the metabolic diversity and specificity of cnidarian – dinoflagellate symbiosis. For this, we combined traditional measurements with nano-scale secondary ion mass spectrometry (NanoSIMS) and stable isotope labeling to investigate carbon and nitrogen cycling both at the organismal scale and the cellular scale. Our results suggest that the individual nutrient assimilation by hosts and symbionts depends on the identity of their respective symbiotic partner. Further, δ^{13}C enrichment patterns revealed that alterations in carbon fixation rates only affected carbon assimilation in the cnidarian host but not the algal symbiont, suggesting a 'selfish' character of this symbiotic association. Based on our findings, we identify new venues for future research regarding the role and regulation of nutrient exchange in the cnidarian - dinoflagellate symbiosis. In this context, the model system approach outlined in this study constitutes a powerful tool set to address these questions.

bioRxiv preprint first posted online Nov. 22, 2017; doi: http://dx.doi.org/10.1101/223933. The copyright holder for this preprint (which was not peer-reviewed) is the author/funder. It is made available under a CC-BY 4.0 International license.

Introduction

Coral reefs thrive in nutrient poor waters (1) and their ecological success fully relies on the nutrient-exchange between cnidarians and dinoflagellate algae of the genus *Symbiodinium* living in the host's tissues (2, 3). In this association, the endosymbiotic algae translocate the majority of their photosynthetically-fixed carbon to the host, which in turn provides inorganic nutrients from its metabolism to sustain algal productivity (2, 4–6). The efficient recycling of organic as well as inorganic nutrients within this symbiosis underpins the high productivity of coral reefs in the absence of major sources of allochthonous nutrients (7, 8). Yet, this ecosystem is in global decline as anthropogenic environmental change impedes the role of cnidarians as key ecosystem engineers (9). Mass bleaching events, i.e. the disruption of cnidarian - dinoflagellate symbiosis signified by the expulsion of symbionts and physical whitening of corals on broad scales, are among the dominant drivers of this decline (10, 11). Understanding the causes of this symbiotic breakdown requires considering these symbiotic organisms as holobionts. Holobionts constitute complex metaorganisms that arise from the interaction of the hosts and their associated microorganisms such as protists, bacteria, and archaea (12). A crucial attribute of cnidarian holobionts is the ability to take up, assimilate, and exchange nutrients (13). In particular, nitrogen cycling appears to be key to the functioning of these holobionts (14, 15), since growth of *Symbiodinium* is nitrogen-limited in a stable symbiosis (14, 16–18). Nitrogen limitation might stabilize symbiont populations and facilitate the translocation of photosynthates to the host (19), a process providing most of the energy required for the host's metabolism (2, 20). Yet, it is unclear whether the host can exert control over this translocation of nutrients (21–23).

Despite the importance of the individual contribution of host and symbionts to holobiont nutrient cycling (14, 23–25), studying these processes in scleractinian corals has proven

bioRxiv preprint first posted online Nov. 22, 2017; doi: http://dx.doi.org/10.1101/223933. The copyright holder for this preprint (which was not peer-reviewed) is the author/funder. It is made available under a CC-BY 4.0 International license.

69 difficult due to the complex and interwoven nature of the coral holobiont. As most corals
70 are associated with a diverse *Symbiodinium* community and cannot be maintained in a
71 symbiont-free stage, identifying underlying processes within these symbiotic interactions is
72 challenging. In contrast, the emerging model organism Aiptasia (*sensu Exaiptasia pallida*
73 (26)) offers distinct advantages to study the cnidarian-dinoflagellate symbiosis (27–29): (I.)
74 this sea anemone can be reared in clonal lines, enabling the study of processes in the
75 absence of biological variation (30); (II.) animals can be maintained in a symbiont-free stage,
76 allowing to study host processes in the absence of symbionts (29); (III.) symbiont-free
77 Aiptasia can be re-infected with specific symbiont strains, enabling the comparison of
78 different symbionts (including those commonly associated with corals) in the same host
79 background *in hospite* (31); (IV.) an extensive array of genetic resources is available in
80 Aiptasia, allowing to link genetic and physiological traits (27). These distinct advantages will
81 prove especially powerful to study metabolic interactions between host and symbionts,
82 particularly if combined with state of the art imaging techniques such as nano-scale
83 secondary ion mass spectrometry (NanoSIMS), which allow precise quantification of
84 element distribution at high spatial resolution (32, 33). Coupled with stable isotope labeling,
85 this technology enables imaging of metabolic processes at subcellular resolution and
86 consequently quantification of nutrients assimilation at the single-cell level for each
87 symbiotic partner (33). NanoSIMS has opened doors to an unprecedented level of
88 information across all fields of biology and has been successfully applied to corals (34–38).
89 In this study, we combined the advantages of the Aiptasia model system with high
90 resolution NanoSIMS to showcase the advantages of this model approach for the study of
91 metabolic interactions and diversity in the cnidarian – dinoflagellate symbiosis.
92

bioRxiv preprint first posted online Nov. 22, 2017; doi: http://dx.doi.org/10.1101/223933. The copyright holder for this preprint (which was not peer-reviewed) is the author/funder. It is made available under a CC-BY 4.0 International license.

Material & methods

Maintenance of Aiptasia

Four different host–symbiont pairings were maintained in separate batches. These combinations involved two different host clonal lines (CC7 (41) and H2 (39)) as well as two different symbiont populations (A4 and B1 dominated (68)). Whilst CC7 Aiptasia can form stable associations with a diversity of *Symbiodinium* types, H2 Aiptasia show high fidelity to their native symbionts suggesting a higher selectivity and/or specificity with their symbionts (40). This specificity of H2 Aiptasia hinders reinfection with other symbionts thereby preventing a full factorial design in this study. Nevertheless, these host clonal lines provide an ideal basis for the comparison of symbiont diversity and specificity.

To allow comparison of symbiont types within the same host line and to compare performance of the same symbiont type within different host lines, CC7 Aiptasia were bleached and reinfected with type B1 (strain SSBO1) symbionts, previously isolated from H2 Aiptasia. For this, non-symbiotic CC7 Aiptasia were generated and reinfected as described by Baumgarten *et al.* (27). In brief, animals were repeatedly bleached by incubation in 4˚C sterile seawater for 4 h, followed by 1-2 days at 25˚C in sterile seawater containing the photosynthesis inhibitor diuron. Non-symbiotic animals were maintained for at least 1 month prior to reinfection to confirm absence of residual symbionts. For reinfection, non-symbiotic animals were subjected to three cycles of incubation for one day in sterile seawater containing 10^5 *Symbiodinium* cells mL^{-1} followed by *Artemia salina* nauplii feeding the next day. Thus, the four combinations were: non-symbiotic CC7 Aiptasia, CC7 Aiptasia with its native A4 symbionts; CC7 Aiptasia reinfected with B1 symbionts and H2 Aiptasia with its native B1 symbionts (Fig. 1A-D). Animals were reared in sterile seawater (35 PSU, 25 °C ,~80 µmol photons m^{-2} s^{-1} on a 12h:12h light:dark schedule) and fed with freshly hatched

bioRxiv preprint first posted online Nov. 22, 2017; doi: http://dx.doi.org/10.1101/223933. The copyright holder for this preprint (which was not peer-reviewed) is the author/funder. It is made available under a CC-BY 4.0 International license.

117 *Artemia salina* nauplii three times per week. Animal cultures were propagated under these
118 conditions for more than one year to ensure anemones recovered from bleaching and
119 reinfection procedures and to confirm the stability of native and introduced symbiotic
120 associations. Stability of *Symbiodinium* communities was monitored using qPCR as outlined
121 by Correa *et al.* (69). Any feeding was abandoned three days prior to measurements to
122 exclude potential confounding effects. Thereby this experimental design allowed us to
123 disentangle the contribution of host and symbionts to holobiont nutrient cycling in three
124 interesting comparisons: (1.) between different symbionts within the same host line, (2.)
125 between different hosts lines with the same symbiont, and (3.) between symbiotic and non-
126 symbiotic states within the same host line.
127
128 *Oxygen flux measurements*
129 Net photosynthesis and respiration rates were measured via oxygen (O_2) evolution and
130 consumption measurements during light and dark incubations, respectively. For this
131 purpose, five specimens of each host–symbiont combination were transferred into 25 ml
132 glass chambers filled with sterile seawater. Specimens were left to settle for 30 min in the
133 dark, before magnetic stirrers were turned on to prevent stratification of the water column.
134 Subsequently, O_2 concentrations were recorded once per second over the course of 30 min
135 incubations during the light (~80 µmol photons m^{-2} s^{-1}, 25˚C) and dark (<1 µmol photons m^{-2}
136 s^{-1}, 25˚C) using FireSting O2 optical oxygen meters (PyroScience, Gemany). Following
137 incubation all specimens were immediately flash frozen and stored at -20˚C until further
138 analysis. Net photosynthesis (inferred from light incubations) as well as respiration (inferred
139 from dark incubations) rates were corrected for seawater controls and normalized to total
140 protein content and *Symbiodinium* densities of specimens. O_2 fluxes of net photosynthesis

bioRxiv preprint first posted online Nov. 22, 2017; doi: http://dx.doi.org/10.1101/223933. The copyright holder for this preprint (which was not peer-reviewed) is the author/funder. It is made available under a CC-BY 4.0 International license.

and respiration rates were transformed into their carbon equivalents using the photosynthetic and respiration quotients of 1.1. and 0.9 as proposed by Muscatine *et al.* (4). Gross photosynthesis rates were calculated according to: gross photosynthesis = net photosynthesis + |respiration| rate.

Quantification of NH_4^+ uptake and release

Net uptake rates were assessed on the holobiont levels during light (~80 µmol photons m^{-2} s^{-1}, 25˚C) and dark (<1 µmol photons m^{-2} s^{-1}, 25˚C) conditions using the depletion technique (70). Five specimens of each host–symbiont combination were incubated for 60 min in 25 ml chambers filled with NH_4^+-enriched artificial seawater (ASW) with a final concentration of 5 µM (71). 10 ml water samples were collected before and after the incubation, filtered (45 µm) and immediately analyzed for ammonium concentrations using an autoanalyzer (SA3000/5000 Chemistry Unit, SKALAR, Netherlands). Differences in NH_4^+ concentrations were corrected for seawater controls and normalized to incubation time, total host protein content and *Symbiodinium* densities of specimens to obtain net uptake rates during both light and dark incubations.

Protein content, Symbiodinium density, and chlorophyll concentrations

Frozen specimens were defrosted in 500 µl sterile saline water and homogenized using a Micro DisTec Homogenizer 125 (Kinematica, Switzerland). Aliquots of the homogenate were immediately analyzed for total protein content as well as symbiont concentrations. For total host protein content, *Symbiodinium* cells were removed by brief centrifugation and the supernatant was analyzed with the Micro BCA Protein Assay Kit (Thermo Scientific, USA) using 150 µl of 15x diluted tissue slurry as per manufacturer instructions. Likewise,

bioRxiv preprint first posted online Nov. 22, 2017; doi: http://dx.doi.org/10.1101/223933. The copyright holder for this preprint (which was not peer-reviewed) is the author/funder. It is made available under a CC-BY 4.0 International license.

163 *Symbiodinium* density was quantified with fluorescence assisted cell sorting (BD
164 LSRFortessa, BD Biosciences, USA) using 100 µl of strained tissue slurry.
165
166 *Isotope labeling and sample preparation*
167 To verify nitrogen and carbon assimilation rates on the holobiont level, an isotopic labeling
168 experiment was conducted for subsequent Nanoscale secondary ion mass spectrometry
169 (NanoSIMS) analysis. Individual specimens of each host–symbiont combination were
170 incubated for 24 h (12h:12 light dark cycle) in 25 ml incubation chambers containing ASW.
171 For isotopic enrichment, freshly prepared ASW, essentially free from bicarbonate and
172 ammonium, was supplemented with $NaH^{13}CO_3$ (isotopic abundance of 99%) as well as
173 $^{15}NH_4Cl$ (isotopic abundance of 99%) at a final concentration of 2mM and 5 µM, respectively
174 (adapted from Harrison *et al.* (71)). Following incubation, all specimens were immediately
175 transferred to a fixative solution (2.5% glutaraldehyde, 1 M cacodylate) and stored at 4˚C
176 until further processing (within 14 days).
177 Individual tentacles were collected from each anemone under a stereomicroscope for
178 further sample preparation adapted after Pernice *et al.* (34) and Kopp *et al.* (46). First,
179 samples were post-fixed for 1h at RT in 1% OsO_4 on Sörensen phosphate buffer (0.1 M).
180 Samples were dehydrated in a serious of increasing ethanol concentrations (50%, 70%, 90%,
181 100%) followed by 100% acetone. Tissues were then gradually infiltrated with SPURR resin
182 of increasing concentrations (25%, 50%, 75%, 100%). Subsequently, tissues were embedded
183 in SPURR resin and cut into 100 nm sections using an Ultracut E microtome (Leica
184 Microsystems, Germany) and mounted on finder grids for Transmission Electron Microscopy
185 (ProsciTech, Australia).
186

bioRxiv preprint first posted online Nov. 22, 2017; doi: http://dx.doi.org/10.1101/223933. The copyright holder for this preprint (which was not peer-reviewed) is the author/funder. It is made available under a CC-BY 4.0 International license.

187 *NanoSIMS imaging*

188 Gold-coated sections were imaged with the NanoSIMS 50 ion probe at the Center for
189 Microscopy, Characterisation and Analysis at the University of Western Australia. Samples
190 surfaces were bombarded with a 16 keV primary Cs^+ beam focused to a spot size of about
191 100 nm, with a current of approximately 2 pA. Secondary molecular ions $^{12}C^{12}C^-$, $^{12}C^{13}C^-$,
192 $^{12}C^{14}N^-$ and $^{12}C^{15}N^-$ were simultaneously collected in electron multipliers at a mass
193 resolution (M/ΔM) of about 8,000, enough to resolve the $^{12}C^{13}C^-$ from the $^{12}C_2{}^1H^-$ peak and
194 the $^{13}C^{14}N^-$ and $^{12}C^{15}N^-$ peaks from one another. Charge compensation was not necessary.
195 Five images of different areas within the gastrodermis of the tentacle (25 - 45 µm raster
196 with 256 × 256 pixels) were recorded for all targeted secondary molecular ions by rastering
197 the primary beam across the sample with a dwell-time of 10-20 ms per pixel. After drift
198 correction, the $^{13}C/^{12}C$ or $^{15}N/^{14}N$ maps were expressed as a hue-saturation-intensity image
199 (HSI), where the color scale represents the isotope ratio. Image processing was performed
200 using the ImageJ plugin OpenMIMS (National Resource for Imaging Mass Spectrometry,
201 https://github.com/BWHCNI/OpenMIMS/wiki).
202 Enrichment of the isotope labels was quantified for 20 ROIs (circles of 2-10 µm) per category
203 (symbiont cells, gastrodermal host tissue and gastrodermal vesicles) for each host–symbiont
204 combination, and expressed using $\delta^{13}C$ and $\delta^{15}N$ notation. Gastrodermal host tissue was
205 quantified in the form for ROIs placed adjacent to symbiont cells as clear cell boundaries
206 were not always identifiable.
207 Unlabeled Aiptasia served as unlabeled controls. $\delta^{13}C$ and $\delta^{15}N$ enrichment was quantified
208 as follows:

209 $$\delta^{13}C = \left(\left(\frac{C_{sample}}{C_{unlabelled}}\right) - 1\right) * 10^3 \text{ and, } \delta^{15}N = \left(\left(\frac{N_{sample}}{N_{unlabelled}}\right) - 1\right) * 10^3$$

bioRxiv preprint first posted online Nov. 22, 2017; doi: http://dx.doi.org/10.1101/223933. The copyright holder for this preprint (which was not peer-reviewed) is the author/funder. It is made available under a CC-BY 4.0 International license.

where N is the $^{15}N/^{14}N$ ratio of sample or unlabeled control and C is the $^{13}C/^{12}C$ ratio (measured as $^{12}C^{13}C^{-}/^{12}C^{12}C^{-}$ ions) of sample or unlabeled control, respectively. In this context, it is important to note that carbon and nitrogen incorporation at the cellular level was likely underestimated in our study as sample preparation for NanoSIMS may result in partial extraction of biomolecules.

Statistical analysis

All statistical analyses were conducted with R version 3.2.2 (72). Data were tested for normal distribution using the Shapiro-Wilk test. All measurements on the holobiont level (gross photosynthesis, respiration, net NH_4^+ uptake) followed normal distribution and were analyzed with a one-way analysis of variance (ANOVA) using host-symbiont combination as explanatory variable; only gross photosynthesis rates normalized by symbiont density did not follow a normal distribution and hence were analyzed with a generalized linear model (GLM) using host-symbiont combination as the explanatory variable. Similarly, $\delta^{13}C$ and $\delta^{15}N$ enrichment data did not follow a normal distribution and were analyzed in two-factorial GLMs using additive as well as interactive effects of host-symbiont combination as well as holobiont compartment (host, lipid body, symbiont). All GLMs were fitted with Gamma distribution and 'log' function to optimize the fit of the model. Fit of model residuals were confirmed using the qqPlot() function as implemented in the 'car' package for R (73). An overview of model results is provided in the Supplementary Information Table S1. Adjustment for multiple comparisons between host-symbiont combinations and holobiont compartments was done following the Bonferroni procedure. Significant differences identified via the post hoc comparison are indicated in the figures as different letters above bars.

bioRxiv preprint first posted online Nov. 22, 2017; doi: http://dx.doi.org/10.1101/223933. The copyright holder for this preprint (which was not peer-reviewed) is the author/funder. It is made available under a CC-BY 4.0 International license.

234

235 **Results**

236 We investigated the relative contribution of cnidarian hosts genotypes and their
237 dinoflagellate symbionts to assimilate dissolved inorganic nitrogen (as ammonium (NH_4^+))
238 and carbon (as bicarbonate) both at the organismal and at the cellular level in Aiptasia by
239 assaying four different associations of hosts and symbionts (Fig. 1A-D). Taken together,
240 these four host–symbiont combinations allowed us to identify nutrient dynamics in
241 symbiotic and non-symbiotic Aiptasia and to address the following questions: (a.) whether
242 different *Symbiodinium* types possess different metabolic capabilities within the same host
243 strain and (b.) to what extent different host strains affect the metabolic performance of the
244 same algal symbiont type.

245

246 *Carbon assimilation and translocation*

247 Host–symbiont combination of Aiptasia showed distinct differences in carbon fixation both
248 at the holobiont (Fig. 1E,G) as well as at the cellular level (Fig. 2A-H, see Supplementary
249 Information Table S1 for an overview of statistical model results). While fixation rates were
250 highly variable between the three groups of symbiotic Aiptasia, no carbon fixation was
251 detectable in non-symbiotic Aiptasia, confirming that carbon assimilation was
252 photosynthetically driven. At the holobiont level, gross carbon fixation (measured as gross
253 photosynthesis) was highest in Aiptasia of the clonal line CC7 with their native symbiont
254 community (*Symbiodinium* type A4) after normalization to symbiont density (Fig. 1E) or host
255 protein content (Fig. 1G). In contrast, CC7 Aiptasia symbiotic with Clade B (SSBO1)
256 *Symbiodinium* showed the lowest gross photosynthesis rates of all symbiotic Aiptasia
257 groupings. In particular, rates were lower than H2 Aiptasia with the same type B1

bioRxiv preprint first posted online Nov. 22, 2017; doi: http://dx.doi.org/10.1101/223933. The copyright holder for this preprint (which was not peer-reviewed) is the author/funder. It is made available under a CC-BY 4.0 International license.

dominated symbiont community. Photosynthetic carbon fixation was more than three-fold higher than dark respiratory carbon consumption in all symbiotic Aiptasia groupings. Overall dark respiration rates followed a less defined yet similar pattern as gross photosynthesis rates of host–symbiont combinations (Supplementary Information Fig. S1A,C), with animal holobionts showing a strong positive correlation between gross photosynthesis and respiration rates (Spearman's correlation, r_s=0.930, p<0.001).

Isotope labeling and NanoSIMS imaging revealed that these observed differences on the holobiont level translated into an intricate picture at the cellular level (Fig. 2A-H). First, δ^{13}C enrichment was evident in both host and symbiont cells in all symbiotic Aiptasia groupings (Fig. 2B-D). Second, although enrichment was highest in *Symbiodinium* cells, localized regions of < 5 µm diameter in the host tissue (referred to as 'lipid bodies' from this point on) also showed significantly higher rates of enrichment compared to the surrounding host tissue. Third, Clade B *Symbiodinium* showed no differences in ^{13}C-incorporation depending on the host, and incorporation rates were 30-40 % lower than in Clade A symbionts. Host lipid bodies, on the contrary, showed a reversed picture with Clade B associated H2 Aiptasia having the highest and Clade B associated CC7 Aiptasia having the lowest ^{13}C assimilation rates, despite harboring the same symbiont types.

NH_4^+ assimilation and release

Similar to carbon fixation, strong differences in ammonium (NH_4^+) assimilation were evident between the experimental groups of Aiptasia at both holobiont ($\chi_{(3,16)} = 87.44$, $p < 0.01$) and cellular levels ($\chi_{(3,352)} = 64.06$, $p < 0.01$). At the holobiont level, all four host—symbiont combinations showed higher NH_4^+ uptake/release rates during the light (Fig. 1F,H), compared to dark conditions (Supplementary Information Fig. S1B,D). When normalized to

bioRxiv preprint first posted online Nov. 22, 2017; doi: http://dx.doi.org/10.1101/223933. The copyright holder for this preprint (which was not peer-reviewed) is the author/funder. It is made available under a CC-BY 4.0 International license.

host protein content, non-symbiotic Aiptasia showed the highest net release of NH_4^+ at the holobiont level both during light (Fig. 1H) and dark incubations (Supplementary Information Fig. S1D). Albeit significantly lower, symbiotic H2 Aiptasia also had a net release of NH_4^+ into the surrounding seawater during the light incubations. In contrast, both groups of symbiotic CC7 Aiptasia showed a net uptake of NH_4^+ by the holobiont during both light and dark conditions. Further, the uptake rate was affected by the associated symbiont community, with Clade A dominated CC7 holobionts taking up more NH_4^+ than their Clade B infected counterparts (Fig. 1F,H).

Although NH_4^+ assimilation ranged from net uptake to net release in the different experimental groups, NanoSIMS imaging confirmed that all four host–symbiont combinations incorporated ^{15}N into their cells (Fig. 2I-P). Whilst $\delta^{15}N$ signatures were highest in *Symbiodinium* cells, ^{15}N assimilation was also observed within the cnidarian host tissue including that of non-symbiotic Aiptasia. Similar to $\delta^{13}C$ patterns, $\delta^{15}N$ enrichment in *Symbiodinium* cells aligned with algal symbiont type rather than host identity, and Clade B symbionts showed lower rates of incorporation than Clade A. Conversely, ^{15}N incorporation into host cells was not significantly different between symbiotic Aiptasia groupings, irrespective of their symbiont type. Non-symbiotic CC7 Aiptasia had the lowest overall ^{15}N incorporation into their tissue, yet showed small (< 5 µm in diameter) and localized regions of high enrichment. In contrast, the afore-mentioned lipid bodies of high $\delta^{13}C$-enrichment showed consistently lower $\delta^{15}N$-signatures than surrounding host tissues in all three symbiotic Aiptasia strains.

Discussion

bioRxiv preprint first posted online Nov. 22, 2017; doi: http://dx.doi.org/10.1101/223933. The copyright holder for this preprint (which was not peer-reviewed) is the author/funder. It is made available under a CC-BY 4.0 International license.

Aiptasia has proven to be a powerful emerging tool for the genetic and molecular study of the cnidarian – alga symbiosis (27, 41, 43). Beyond these realms, only few studies have begun to exploit the advantages that Aiptasia has to offer (24, 25, 44, 45). Here, we set out to assess the use of Aiptasia as a model to study nutrient cycling in the cnidarian – alga symbiosis. Whilst NanoSIMS has been successfully used previously to study nutrient uptake in corals (46–48), the flexibility of the Aiptasia model enables for the first time to decouple the relative contribution of the host and symbionts to nutrient cycling. Although the methodology outlined in our approach was optimized to trace carbon and nitrogen assimilation within coral or Aiptasia holobiont (34, 46), the method can be easily modified depending on the experimental requirements. Specific labeled compounds can also be used as tracers to follow the translocation and uptake of specific molecules in complex systems by coupling the spatial resolution of NanoSIMS with the molecular characterization afforded by time-of-flight secondary ion mass spectrometry (ToF-SIMS) (49). Also, as shown here, detailed cellular insights gained from NanoSIMS will prove most powerful when integrated with traditional holobiont based measurements to identify the complexity of processes. Using this integrative approach, differences in nutrient assimilation across different host–symbiont associations became evident, both at the holobiont as well as the cellular level. Yet, only the integration of both levels of biological organization allowed to comprehensively disentangle some of the intricacies of nutrient cycling in the Aiptasia holobiont.

Carbon cycling in Aiptasia

All three groups of symbiotic Aiptasia showed high rates of gross photosynthesis that exceeded their respiratory carbon requirements thereby supporting net productivity of the

bioRxiv preprint first posted online Nov. 22, 2017; doi: http://dx.doi.org/10.1101/223933. The copyright holder for this preprint (which was not peer-reviewed) is the author/funder. It is made available under a CC-BY 4.0 International license.

329 holobiont required for stable symbiotic associations (4). Yet, differences in gross
330 photosynthesis between host–symbiont combinations were evident at the holobiont level.
331 Gross photosynthesis rates differed between the same host infected with different algal
332 symbionts and between different hosts infected with the same algal symbionts. Thereby our
333 findings support the findings by Stazark *et al.* (24) who reported differences in carbon flux
334 depending on symbiont type and between heterologous and homologous symbionts in
335 Aiptasia, confirming previous observations that carbon fixation depends on the interaction
336 of both host and symbionts (24, 25, 36, 50).
337 At the cellular level, we observed particular areas of δ^{13}C enrichment (hotspots) in the host
338 tissue similar to previous observations (36, 51). This high δ^{13}C enrichment is further coupled
339 with lower δ^{15}N enrichment, suggesting that these hotspots likely constitute a form of
340 carbon storage compartments in the host tissue. Based on shape, size, and location in the
341 tissue, these compartments are most likely lipid bodies (52). These cellular organelles are
342 abundant in symbiotic cnidarians as they allow for rapid short-term carbon storage and
343 remobilization depending on cellular carbon availability (53). Hence, amount, size and
344 enrichment of these lipid bodies may be an excellent proxy to assess the amount of carbon
345 translocated by *Symbiodinium* to the host, but further studies are needed to unequivocally
346 determine their nature. Lipid body enrichment in the host was highest in H2 Aiptasia and
347 lowest in CC7 Aiptasia, both associated with *Symbiodinium* type B1. Yet, δ^{13}C enrichment in
348 algal cells was unaffected by host identity. At the same time, our results revealed that Clade
349 A and B symbionts had distinctly different δ^{13}C enrichment, even in the same clonal Aiptasia
350 host line. These differences are likely the consequence of differential metabolic
351 requirements by the specific symbionts. Thus, δ^{13}C enrichment may be a powerful tool to
352 differentiate between symbiont types *in hospite*.

bioRxiv preprint first posted online Nov. 22, 2017; doi: http://dx.doi.org/10.1101/223933. The copyright holder for this preprint (which was not peer-reviewed) is the author/funder. It is made available under a CC-BY 4.0 International license.

353 Taken together, observed differences in gross carbon fixation at the holobiont level were
354 reflected in the combined δ^{13}C enrichment (host tissue + lipid bodies + symbionts) at the
355 cellular level. However, NanoSIMS data revealed that these patterns were only caused by
356 differences in enrichment of the host lipid bodies (a proxy of carbon translocation to the
357 host). In contrast, δ^{13}C enrichment in algal cells differed depending on symbiont type (i.e.,
358 showed stable δ13C enrichment within the same symbiont types), but was unaffected by
359 host identity. This apparent contradiction may have important implications for our
360 understanding of symbiosis functioning. The fact that δ13C enrichment in algal cells differed
361 only depending on symbiont type but was unaffected by host identity implies that
362 symbionts retained the same amount of fixed carbon regardless of overall fixed carbon
363 availability. Hence, only excess carbon, not consumed by algal metabolism, appears to be
364 available for translocation to the host. Therefore, factors reducing the availability of excess
365 carbon in the symbiont, may potentially deprive the host of its main energy source, despite
366 harboring viable symbionts in its tissue. This 'selfish' aspect of the symbiosis may pose a
367 potential threat to the stability of the holobiont under conditions of reduced fixed-carbon
368 availability, such as those imposed by environmental stress (54, 55).
369
370 *Nitrogen cycling in Aiptasia*
371 The observation of drastically different carbon fixation and translocation rates between
372 different host–symbiont combinations raises questions regarding the underlying regulatory
373 mechanisms of carbon cycling within these symbioses (13). Importantly, nitrogen availability
374 *in hospite* has been proposed to be among the environmental controls of these processes
375 (14, 15, 19, 56). Indeed, drastic differences in nitrogen assimilation became evident when
376 comparing different host–symbiont combinations. Strikingly, the two different host lines

bioRxiv preprint first posted online Nov. 22, 2017; doi: http://dx.doi.org/10.1101/223933. The copyright holder for this preprint (which was not peer-reviewed) is the author/funder. It is made available under a CC-BY 4.0 International license.

377 Aiptasia H2 and CC7 showed net NH_4^+ release and NH_4^+ uptake during the light, respectively,
378 even when hosting the same algal symbionts. These findings suggest that the *in hospite*
379 nutrient availability for the symbiont may be drastically different depending on the
380 associated Aiptasia host. Hence, differences in gross photosynthetic activity and
381 translocation may be partly attributed to variations in availability of nitrogen derived from
382 the host metabolism. Interestingly, while CC7 Aiptasia showed light-enhanced NH_4^+ uptake
383 as previously reported for corals (57), H2 Aiptasia showed net release of NH_4^+ during the
384 light, contrasted by slight uptake during the dark. While we cannot explain this discrepancy
385 at this point, it illustrates the drastic effects of host identity on nitrogen assimilation of the
386 holobiont. At any rate, our results highlight the functional diversity and specificity of
387 cnidarian-dinoflagellate symbioses, prompting research across a range of host–symbiont
388 combinations.
389 At this point it is not possible to distinguish whether the increased $\delta^{15}N$ enrichment of host
390 tissues in symbiotic animals are due to direct NH_4^+ fixation by the host or the translocation
391 of fixed nitrogen by the symbiont. However, nitrogen assimilation was observed even in the
392 absence of algal symbionts, as evidenced by non-symbiotic Aiptasia. Although these animals
393 showed a high net release of NH_4^+ at the holobiont level, NanoSIMS imaging confirmed the
394 incorporation of ^{15}N within localized hotspots of their tissue at low rates. While the exact
395 nature of these hotspots remains unknown at this point, our results confirm that Aiptasia
396 also has the ability to assimilate inorganic nitrogen from seawater as previously reported for
397 corals (34). However, it remains to be determined whether this capability is intricate to the
398 host cellular machinery or a function of associated bacterial symbionts or both (48).
399 In contrast to $\delta^{15}N$ enrichment of their hosts, *Symbiodinium* types showed characteristic
400 $\delta^{15}N$ enrichment patterns regardless of the identity of their host. Hence, $\delta^{15}N$ enrichment

bioRxiv preprint first posted online Nov. 22, 2017; doi: http://dx.doi.org/10.1101/223933. The copyright holder for this preprint (which was not peer-reviewed) is the author/funder. It is made available under a CC-BY 4.0 International license.

401 may prove a useful tool to identify symbiont identity *in hospite*, especially when combined
402 with δ^{13}C measurements.
403 Different to carbon fixation measurement, patterns of NH_4^+ uptake on the holobiont level
404 were not directly reflected in the overall δ^{15}N enrichment on the cellular level. Specifically,
405 symbiont-free CC7 Aiptasia as well as symbiotic H2 Aiptasia showed net release of NH_4^+
406 from the holobiont during light conditions, yet NanoSIMS analysis confirmed the
407 incorporation of ^{15}N from surrounding seawater. While these differences may be partly
408 attributed to differences in incubation time and light availability for the two measurements,
409 they further suggest that uptake and release of NH_4^+ appear to be in a dynamic equilibrium
410 in Aiptasia. Hence, the stable δ^{15}N enrichment of the same symbiont type in CC7 and H2
411 suggests that the contribution of nitrogen derived from host metabolism was negligible
412 compared to the incorporation of nitrogen from seawater under these conditions. Under
413 natural oligotrophic conditions, however, host metabolism may make a significant
414 contribution to the nitrogen supply of the symbiont.
415
416 *Deciphering the role of nutrient cycling in cnidarian holobionts*
417 Our results suggest (I.) that nutrient cycling is drastically altered between symbiotic and
418 non-symbiotic Aiptasia; (II.) that different *Symbiodinium* types possess different metabolic
419 capabilities within the same Aiptasia strain and (III.) that different Aiptasia strains affect the
420 metabolic performance of the same algal symbiont. Although our results require further
421 validation with regard to their wider applicability beyond the Aiptasia model system, our
422 findings showcase the distinct advantages of a model system approach for the study of
423 nutrient cycling in the the cnidarian – dinoflagellate symbiosis. However, questions remain
424 regarding the precise nature of nutrients exchanged in this symbiosis and the underlying

bioRxiv preprint first posted online Nov. 22, 2017; doi: http://dx.doi.org/10.1101/223933. The copyright holder for this preprint (which was not peer-reviewed) is the author/funder. It is made available under a CC-BY 4.0 International license.

425 processes involved. Since nutrient exchange is arguably the functional basis of mutualistic
426 association (7), providing answers to these questions is one of the keys to understanding
427 holobiont functioning (14). Furthermore, nutrient cycling is likely a dominant driver of
428 holobiont fitness under varying environmental conditions (58–61). Understanding
429 environmental controls of nutrient cycling may therefore help to provide novel insights on
430 the mechanisms of symbiosis establishment, maintenance, and disruption.
431 In this context, we formulate three important questions that are relevant for future studies
432 of nutrient cycling in cnidarian holobionts:
433 **(I.) How does symbiont diversity affect nutrient exchange within the symbiosis and how**
434 **does it influence holobiont success under varying environmental conditions?** It has been
435 previously observed that the performance of symbionts depends on the environmental
436 conditions (e.g. during coral bleaching) (62). While many studies have investigated the role
437 of oxidative stress in these phenomena (63, 64), nutrient cycling is likely another important
438 factor involved.
439 **(II.) How is nutrient cycling regulated during symbiosis establishment and maintenance?** In
440 contrast to mature coral holobionts, carbon translocation by symbionts appears to be
441 negligible in early stages of symbiosis establishment (51, 65). Understanding the processes
442 around initiating and stabilizing this nutrient exchange during symbiosis development will
443 advance our understanding of the factors underlying the success of this symbiosis.
444 **(III.) What is the role of bacteria and other microbes in holobiont nutrient cycling?** It is
445 widely acknowledged that carbon, nitrogen, and sulfur cycling microbes are ubiquitous
446 members of the cnidarian microbiome (32, 66, 67). However, questions remain regarding
447 their relevance and contribution to holobiont function. Studying nutrient exchange between

bioRxiv preprint first posted online Nov. 22, 2017; doi: http://dx.doi.org/10.1101/223933. The copyright holder for this preprint (which was not peer-reviewed) is the author/funder. It is made available under a CC-BY 4.0 International license.

448 these microbes and other members of the holobiont is necessary to evaluate the
449 importance of the microbiome for holobiont fitness.
450 Future research efforts incorporating a model system approach with field-based coral
451 studies, will transform our understanding of the mechanisms underlying this symbiosis and
452 may prompt new solutions to prevent further loss and degradation of reef ecosystem.
453

454 **Conflict of interest**

455 None declared.
456

457 **Author contributions**

458 NR, MA and CRV conceived and designed the experiment. NR, JBR, MP and GP conducted
459 the experiment. PG and MRK carried out NanoSIMS data acquisition. All authors wrote,
460 revised and approved the manuscript.
461

462 **Funding**

463 - KAUST AIMS CPF partnership funding to CRV & NR.
464 - KAUST baseline research funds to CRV.
465 - Australian Microscopy & Microanalysis Research Facility, AuScope, the Science and
466 Industry Endowment Fund, and the State Government of Western Australian
467 contributed to the Ion Probe Facility at the Centre for Microscopy, Characterisation
468 and Analysis at the University of Western Australia.
469 - Australian Research Council fellowship DE160100636 to JBR.
470

471 **Acknowledgements**

bioRxiv preprint first posted online Nov. 22, 2017; doi: http://dx.doi.org/10.1101/223933. The copyright holder for this preprint (which was not peer-reviewed) is the author/funder. It is made available under a CC-BY 4.0 International license.

The authors would like to thank Dr. Rachid Sougrat and Ptissam Bergam from the KAUST imaging core lab for their help with sample preparation. CRV and NR acknowledge funding from the KAUST AIMS CPF partnership funding. Further, research in this publication was supported by KAUST baseline research funds to CRV. The authors would like to acknowledge the Australian Microscopy & Microanalysis Research Facility, AuScope, the Science and Industry Endowment Fund, and the State Government of Western Australian for contributing to the Ion Probe Facility at the Centre for Microscopy, Characterisation and Analysis at the University of Western Australia. JBR was supported by Australian Research Council fellowship DE160100636.

bioRxiv preprint first posted online Nov. 22, 2017; doi: http://dx.doi.org/10.1101/223933. The copyright holder for this preprint (which was not peer-reviewed) is the author/funder. It is made available under a CC-BY 4.0 International license.

References

1. **Hatcher BG**. 1988. Coral reef primary productivity: a beggar's banquet. Trends Ecol Evol **3**:106–11.

2. **Falkowski PPG**, **Dubinsky Z**, **Muscateine L**, **Porter JJW**. 1984. Light and bioenergetics of a symbiotic coral. Bioscience **34**:705–709.

3. **Hatcher BG**. 1997. Coral reef ecosystems: how much greater is the whole than the sum of the parts? Coral Reefs **16**:77–91.

4. **Muscatine L**, **McCloskey LR**, **Marian RE**. 1981. Estimating the daily contribution of carbon from zooxanthellae to coral animal respiration. Limnol Oceanogr **26**:601–611.

5. **Muscatine L**. 1967. Glycerol excretion by symbiotic algae from corals and *Tridacna* and its control by the host. Science (80-) **156**:516–519.

6. **Rädecker N**, **Pogoreutz C**, **Wild C**, **Voolstra CR**. 2017. Stimulated respiration and net photosynthesis in $_{Cassiopeia}$ sp. during glucose enrichment suggests in hospite CO_2 limitation of algal endosymbionts. Front Mar Sci **4**:267.

7. **Muscatine L**, **Porter JW**. 1977. Reef corals: mutualistic symbioses adapted to nutrient-poor environments. Bioscience **27**:454–460.

8. **Wang JT**, **Douglas AE**. 1998. Nitrogen recycling or nitrogen conservation in an alga-invertebrate symbiosis? J Exp Biol **201**:2445–2453.

9. **Wild C**, **Hoegh-Guldberg O**, **Naumann MS**, **Colombo-Pallotta F**, **Ateweberhan M**, **Fitt WK**, **Iglesias-Prieto R**, **Palmer C**, **Bythell JC**, **Ortiz J**, **Loya Y**, **van Woesik R**. 2011. Climate change impedes scleractinian corals as primary reef ecosystem engineers. Mar Freshw Res **62**:205–215.

10. **Bellwood DR**, **Hughes TP**, **Folke C**, **Nyström M**. 2004. Confronting the coral reef crisis. Nature **429**:827–33.

11. **Hughes TP**, **Kerry J**, **Álvarez-Noriega M**, **Álvarez-Romero J**, **Anderson K**, **Baird A**, **Babcock R**, **Beger M**, **Bellwood D**, **Berkelmans R**, **Bridge T**, **Butler I**, **Byrne M**, **Cantin N**, **Comeau S**, **Connolly S**, **Cumming G**, **Dalton S**, **Diaz-Pulido G**, **Eakin CM**, **Figueira W**, **Gilmour J**, **Harrison H**, **Heron S**, **Hoey AS**, **Hobbs J-P**, **Hoogenboom M**, **Kennedy E**, **Kuo C-Y**, **Lough J**, **Lowe R**, **Liu G**, **Malcolm McCulloch HM**, **McWilliam M**, **Pandolfi J**, **Pears R**, **Pratchett M**, **Schoepf V**, **Simpson T**, **Skirving W**, **Sommer B**, **Torda G**, **Wachenfeld D**, **Willis B**, **Wilson S**. 2017. Global warming and recurrent mass bleaching of corals. Nature **543**:373–377.

12. **Rosenberg E**, **Koren O**, **Reshef L**, **Efrony R**, **Zilber-Rosenberg I**. 2007. The role of microorganisms in coral health, disease and evolution. Nat Rev Microbiol **5**:355–62.

13. **Suggett DJ**, **Warner ME**, **Leggat W**. 2017. Symbiotic dinoflagellate functional diversity mediates coral survival under ecological crisis. Trends Ecol Evol.

bioRxiv preprint first posted online Nov. 22, 2017; doi: http://dx.doi.org/10.1101/223933. The copyright holder for this preprint (which was not peer-reviewed) is the author/funder. It is made available under a CC-BY 4.0 International license.

518 14. **Rädecker N**, **Pogoreutz C**, **Voolstra CR**, **Wiedenmann J**, **Wild C**. 2015. Nitrogen
519 cycling in corals: The key to understanding holobiont functioning? Trends Microbiol
520 **23**:490–497.

521 15. **Pogoreutz C**, **Rädecker N**, **Cárdenas A**, **Gärdes A**, **Voolstra CR**, **Wild C**. 2017.
522 Sugar enrichment provides evidence for a role of nitrogen fixation in coral bleaching.
523 Glob Chang Biol **23**: 3838-3848.

524 16. **Falkowski PG**, **Dubinsky Z**, **Muscatine L**, **McCloskey L**. 1993. Population control
525 in symbiotic corals. Bioscience **43**:606–611.

526 17. **Muscatine L**, **Falkowski PG**, **Dubinsky PA**, **Cook CA**, **McCloskey LRR**, **Falkowsk**
527 **PG**, **Dubinsky Z**, **Cook PA**, **McCloskey LRR**. 1989. The effect of external nutrient
528 resources on the population dynamics of zooxanthellae in a reef coral. Proc R Soc
529 London Ser B Biol Sci **236**:311–324.

530 18. **Belda CA**, **Lucas JS**, **Yellowlees D**. 1993. Effects of nutrient supplements on growth
531 of the symbiotic partners. Mar Biol **664**:655–664.

532 19. **Ezzat L**, **Maguer J-F**, **Grover R**, **Ferrier-Pagès C**. 2015. New insights into carbon
533 acquisition and exchanges within the coral – dinoflagellate symbiosis under NH_4^+ and
534 NO_3^- supply. Proc R Soc B Biol Sci **282**:20150610.

535 20. **Tremblay P**, **Grover R**, **Maguer JF**, **Legendre L**, **Ferrier-Pagès C**. 2012.
536 Autotrophic carbon budget in coral tissue: a new ^{13}C-based model of photosynthate
537 translocation. J Exp Biol **215**:1384–93.

538 21. **Wooldridge SA**. 2010. Is the coral-algae symbiosis really “mutually beneficial” for
539 the partners? BioEssays **32**:615–25.

540 22. **Jones RJ**, **Yellowlees D**. 1997. Regulation and control of intracellular algae (=
541 zooxanthellae) in hard corals. Philos Trans R Soc B Biol Sci **352**:457–468.

542 23. **Yellowlees D**, **Rees TA**, **Leggat W**. 2008. Metabolic interactions between algal
543 symbionts and invertebrate hosts. Plant Cell Environ **31**:679–694.

544 24. **Starzak DE**, **Quinnell RG**, **Nitschke MR**, **Davy SK**. 2014. The influence of
545 symbiont type on photosynthetic carbon flux in a model cnidarian-dinoflagellate
546 symbiosis. Mar Biol **161**:711–724.

547 25. **Leal MC**, **Hoadley K**, **Pettay DT**, **Grajales A**, **Calado R**, **Warner ME**. 2015.
548 Symbiont type influences trophic plasticity of a model cnidarian-dinoflagellate
549 symbiosis. J Exp Biol **218**:858–863.

550 26. **Grajales A**, **RodrÍguez E**. 2014. Morphological revision of the genus *Aiptasia* and the
551 family Aiptasiidae (Cnidaria, Actiniaria, Metridioidea). Zootaxa **3826**:55–100.

552 27. **Baumgarten S**, **Simakov O**, **Esherick LY**, **Jin Y**, **Lehnert EM**, **Michell CT**, **Li Y**,
553 **Pringle JR**, **Voolstra CR**. 2015. The genome of *Aiptasia*, a sea anemone model for

bioRxiv preprint first posted online Nov. 22, 2017; doi: http://dx.doi.org/10.1101/223933. The copyright holder for this preprint (which was not peer-reviewed) is the author/funder. It is made available under a CC-BY 4.0 International license.

554 coral symbiosis. Proceeding Natl Acad Sci United States Am **112**:11893–11898.

555 28. **Röthig T**, **Costa RM**, **Simona F**, **Baumgarten S**, **Torres AF**, **Radhakrishnan A**,
556 **Aranda M**, **Voolstra CR**. 2016. Distinct bacterial communities associated with the
557 coral model *Aiptasia* in aposymbiotic and symbiotic states with Symbiodinium. Front
558 Mar Sci **3**:234.

559 29. **Voolstra CR**. 2013. A journey into the wild of the cnidarian model system *Aiptasia*
560 and its symbionts. Mol Ecol **22**:4366–4368.

561 30. **Weis VM**, **Davy SK**, **Hoegh-Guldberg O**, **Rodriguez-Lanetty M**, **Pringle JR**. 2008.
562 Cell biology in model systems as the key to understanding corals. Trends Ecol Evol
563 **23**:369–376.

564 31. **Wolfowicz I**, **Baumgarten S**, **Voss PA**, **Hambleton EA**, **Voolstra CR**, **Hatta M**,
565 **Guse A**. 2016. *Aiptasia* sp. larvae as a model to reveal mechanisms of symbiont
566 selection in cnidarians. Sci Rep **6**:srep32366.

567 32. **Neave MJ**, **Apprill A**, **Ferrier-Pages C**, **Voolstra CR**. 2016. Diversity and function
568 of prevalent symbiotic marine bacteria in the genus *Endozoicomonas*. Appl Microbiol
569 Biotechnol **100**:8315–8324.

570 33. **Pernice M**, **Levy O**. 2014. Novel tools integrating metabolic and gene function to
571 study the impact of the environment on coral symbiosis. Front Microbiol **5**:448.

572 34. **Pernice M**, **Meibom A**, **Van Den Heuvel A**, **Kopp C**, **Domart-Coulon I**, **Hoegh-**
573 **Guldberg O**, **Dove S**. 2012. A single-cell view of ammonium assimilation in coral-
574 dinoflagellate symbiosis. ISME J **6**:1314–24.

575 35. **Kopp C**, **Pernice M**, **Domart-Coulon I**, **Djediat C**, **Spangenberg JE**, **Alexander D**,
576 **Hignette M**, **Meziane T**, **Meibom A**. 2013. Highly dynamic cellular-level response of
577 symbiotic coral to a sudden increase in environmental nitrogen. MBio **4**:e00052-13.

578 36. **Pernice M**, **Dunn SR**, **Tonk L**, **Dove S**, **Domart-Coulon I**, **Hoppe P**, **Schintlmeister**
579 **A**, **Wagner M**, **Meibom A**. 2014. A nanoscale secondary ion mass spectrometry study
580 of dinoflagellate functional diversity in reef-building corals. Environ Microbiol
581 **17**:3570–3580.

582 37. **Lechene CP**, **Luyten Y**, **McMahon G**, **Distel DL**. 2007. Quantitative imaging of
583 nitrogen fixation by individual bacteria within animal cells. Science **317**:1563–1566.

584 38. **Musat N**, **Musat F**, **Weber PK**, **Pett-Ridge J**. 2016. Tracking microbial interactions
585 with NanoSIMS. Curr Opin Biotechnol **41**:114–121.

586 39. **Xiang T**, **Hambleton EA**, **Denofrio JC**, **Pringle JR**, **Grossman AR**. 2013. Isolation
587 of clonal axenic strains of the symbiotic dinoflagellate Symbiodinium and their growth
588 and host specificity. J Phycol **49**:447–458.

589 40. **Thornhill DJ**, **Xiang Y**, **Pettay DT**, **Zhong M**, **Santos SR**. 2013. Population genetic

bioRxiv preprint first posted online Nov. 22, 2017; doi: http://dx.doi.org/10.1101/223933. The copyright holder for this preprint (which was not peer-reviewed) is the author/funder. It is made available under a CC-BY 4.0 International license.

data of a model symbiotic cnidarian system reveal remarkable symbiotic specificity and vectored introductions across ocean basins. Mol Ecol **22**:4499–4515.

41. **Sunagawa S**, **Wilson EC**, **Thaler M**, **Smith ML**, **Caruso C**, **Pringle JR**, **Weis VM**, **Medina M**, **Schwarz JA**. 2009. Generation and analysis of transcriptomic resources for a model system on the rise: the sea anemone *Aiptasia pallida* and its dinoflagellate endosymbiont. BMC Genomics **10**:258.

42. **Bieri T**, **Onishi M**, **Xiang T**, **Grossmann AR**, **Pringle JR**. 2016. Relative contributions of various cellular mechanisms to loss of algae during cnidarian bleaching. PLoS One **11**:e0152693.

43. **Bellis ES**, **Howe DK**, **Denver DR**. 2016. Genome-wide polymorphism and signatures of selection in the symbiotic sea anemone Aiptasia. BMC Genomics **17**:160.

44. **Biquand E**, **Okubo N**, **Aihara Y**, **Rolland V**, **Hayward DC**, **Hatta M**, **Minagawa J**, **Maruyama T**, **Takahashi S**. 2017. Acceptable symbiont cell size differs among cnidarian species and may limit symbiont diversity. ISME J **11**:1702-1712.

45. **Tolleter D**, **Seneca FO**, **Denofrio JC**, **Krediet CJ**, **Palumbi SR**, **Pringle JR**, **Grossman AR**. 2013. Coral bleaching independent of photosynthetic activity. Curr Biol **23**:1782–1786.

46. **Kopp C**, **Domart-Coulon I**, **Escrig S**, **Humbel BM**, **Hignette M**, **Meibom A**. 2015. Subcellular investigation of photosynthesis-driven carbon and nitrogen assimilation and utilization in the symbiotic reef coral *Pocillopora damicornis*. mBio **6**:e02299-14.

47. **Lema KA**, **Clode PL**, **Kilburn MR**, **Thornton R**, **Willis BL**, **Bourne DG**. 2016. Imaging the uptake of nitrogen-fixing bacteria into larvae of the coral Acropora millepora. ISME J **10**:18084–1808.

48. **Ceh J**, **Kilburn MR**, **Cliff JB**, **Raina J-B**, **van Keulen M**, **Bourne DG**. 2013. Nutrient cycling in early coral life stages: *Pocillopora damicornis* larvae provide their algal symbiont (*Symbiodinium*) with nitrogen acquired from bacterial associates. Ecol Evol **3**:2393–2400.

49. **Raina JB**, **Clode P**, **Cheong S**, **Bougoure J**, **Kilburn MR**, **Reeder A**, **Forêt S**, **Stat M**, **Beltran V**, **Thomas-Hall P**, **Tapiolas D**, **Motti CM**, **Gong B**, **Pernice M**, **Marjo CE**, **Seymour JR**, **Willis BL**, **Bourne DG**. 2017. Subcellular tracking reveals the location of dimethylsulfoniopropionate in microalgae and visualises its uptake by marine bacteria. elife **6**:e23008.

50. **Goulet TL**, **Cook CB**, **Goulet D**. 2005. Effect of short-term exposure to elevated temperatures and light levels on photosynthesis of different host-symbiont combinations in the *Aiptasia pallida-Symbiodinium* symbiosis. Limnol Oceanogr **50**:1490–1498.

51. **Kopp C**, **Domart-Coulon I**, **Barthelemy D**, **Meibom A**. 2016. Nutritional input from

bioRxiv preprint first posted online Nov. 22, 2017; doi: http://dx.doi.org/10.1101/223933. The copyright holder for this preprint (which was not peer-reviewed) is the author/funder. It is made available under a CC-BY 4.0 International license.

627 dinoflagellate symbionts in reef-building corals is minimal during planula larval life
628 stage. Sci Adv **2**:e1500681.

629 52. **Peng SE**, **Chen WNU**, **Chen HK**, **Lu CY**, **Mayfield AB**, **Fang LS**, **Chen CS**. 2011.
630 Lipid bodies in coral-dinoflagellate endosymbiosis: Proteomic and ultrastructural
631 studies. Proteomics **11**:3540–3555.

632 53. **Chen WNU**, **Kang HJ**, **Weis VM**, **Mayfield AB**, **Jiang PL**, **Fang LS**, **Chen CS**.
633 2012. Diel rhythmicity of lipid-body formation in a coral-*Symbiodinium*
634 endosymbiosis. Coral Reefs **31**:521–534.

635 54. **Anthony KRN**, **Hoogenboom MO**, **Maynard JA**, **Grottoli AG**, **Middlebrook R**.
636 2009. Energetics approach to predicting mortality risk from environmental stress: A
637 case study of coral bleaching. Funct Ecol **23**:539–550.

638 55. **Anthony KRN**, **Kline DI**, **Diaz-Pulido G**, **Dove S**, **Hoegh-Guldberg O**. 2008. Ocean
639 acidification causes bleaching and productivity loss in coral reef builders. Proceeding
640 Natl Acad Sci United States Am **105**:17442–17446.

641 56. **Wooldridge SA**. 2013. Breakdown of the coral-algae symbiosis: towards formalising
642 a linkage between warm-water bleaching thresholds and the growth rate of the
643 intracellular zooxanthellae. Biogeosciences **10**:1647–1658.

644 57. **Grover R**, **Maguer J-F**, **Vaganay SR-**, **S CF-P**, **Reynaud-vaganay S**, **Ferrier-page**
645 **C**. 2002. Uptake of ammonium by the scleractinian coral *Stylophora pistillata*: effect
646 of feeding, light, and ammonium concentrations. Limnol Oceanogr **47**:782–790.

647 58. **Wiedenmann J**, **D'Angelo C**, **Smith EG**, **Hunt AN**, **Legiret F-E**, **Postle AD**,
648 **Achterberg EP**. 2012. Nutrient enrichment can increase the susceptibility of reef
649 corals to bleaching. Nat Clim Chang **2**:1–5.

650 59. **Wooldridge SA**, **Done TJ**. 2009. Improved water quality can ameliorate effects of
651 climate change on corals. Ecol Appl **19**:1492–1499.

652 60. **Ferrier-Pagès C**, **Godinot C**, **D'Angelo C**, **Wiedenmann J**, **Grover R**. 2016.
653 Phosphorus metabolism of reef organisms with algal symbionts. Ecol Monogr **86**:262–
654 277.

655 61. **Ezzat L**, **Maguer J-F**, **Grover R**, **Ferrier-Pagès C**. 2016. Limited phosphorus
656 availability is the Achilles heel of tropical reef corals in a warming ocean. Sci Rep
657 **6**:31768.

658 62. **Silverstein RN**, **Cunning R**, **Baker AC**. 2014. Change in algal symbiont communities
659 after bleaching, not prior heat exposure, increases heat tolerance of reef corals. Glob
660 Chang Biol 236–249.

661 63. **McGinty ES**, **Pieczonka J**, **Mydlarz LD**. 2012. Variations in reactive oxygen release
662 and antioxidant activity in multiple *Symbiodinium* types in response to elevated
663 temperature. Microb Ecol **64**:1000–1007.

bioRxiv preprint first posted online Nov. 22, 2017; doi: http://dx.doi.org/10.1101/223933. The copyright holder for this preprint (which was not peer-reviewed) is the author/funder. It is made available under a CC-BY 4.0 International license.

64. **Tchernov D**, **Gorbunov MY**, **de Vargas C**, **Narayan Yadav S**, **Milligan AJ**, **Häggblom M**, **Falkowski PG**. 2004. Membrane lipids of symbiotic algae are diagnostic of sensitivity to thermal bleaching in corals. Proc Natl Acad Sci U S A **101**:13531–13535.

65. **Mies M**, **Sumida PYG**, **Rädecker N**, **Voolstra CR**. 2017. Marine invertebrate larvae associated with *Symbiodinium*: A mutualism from the start? Front Ecol Evol **5**:56.

66. **Raina J-B**, **Dinsdale EA**, **Willis BL**, **Bourne DG**. 2010. Do the organic sulfur compounds DMSP and DMS drive coral microbial associations? Trends Microbiol **18**:101–8.

67. **Lema KA**, **Willis BL**, **Bourne DG**. 2012. Corals form characteristic associations with symbiotic nitrogen-fixing bacteria. Appl Environ Microbiol **78**:3136–3144.

68. **Grawunder D**, **Hambleton EA**, **Bucher M**, **Wolfowicz I**, **Bechtoldt N**, **Guse A**. 2015. Induction of gametogenesis in the cnidarian endosymbiosis model *Aiptasia* sp. Sci Rep **5**:15677.

69. **Correa AMS**, **McDonald MD**, **Baker AC**. 2009. Development of clade-specific *Symbiodinium* primers for quantitative PCR (qPCR) and their application to detecting clade D symbionts in Caribbean corals. Mar Biol **156**:2403–2411.

70. **Godinot C**, **Grover R**, **Allemand D**, **Ferrier-Pagès C**. 2011. High phosphate uptake requirements of the scleractinian coral *Stylophora pistillat*a. J Exp Biol **214**:2749–2754.

71. **Harrison PJ**, **Waters RE**, **Taylor FJR**. 1980. A broad spectrum artificial sea water medium for coastal and open ocean phytoplankton. J Phycol **16**:28–35.

72. **R Development Core Team R**, **Team RC**. 2015. R: A language and environment for statistical computing. R Found Stat Comput. R Foundation for Statistical Computing, Vienna, Austria.

73. **John A**, **Fox I**, **Bates D**, **Firth D**, **Friendly M**, **Monette G**, **Ripley B**, **Weisberg S**. 2003. The car Package. Source.

bioRxiv preprint first posted online Nov. 22, 2017; doi: http://dx.doi.org/10.1101/223933. The copyright holder for this preprint (which was not peer-reviewed) is the author/funder. It is made available under a CC-BY 4.0 International license.

692 **Figures**

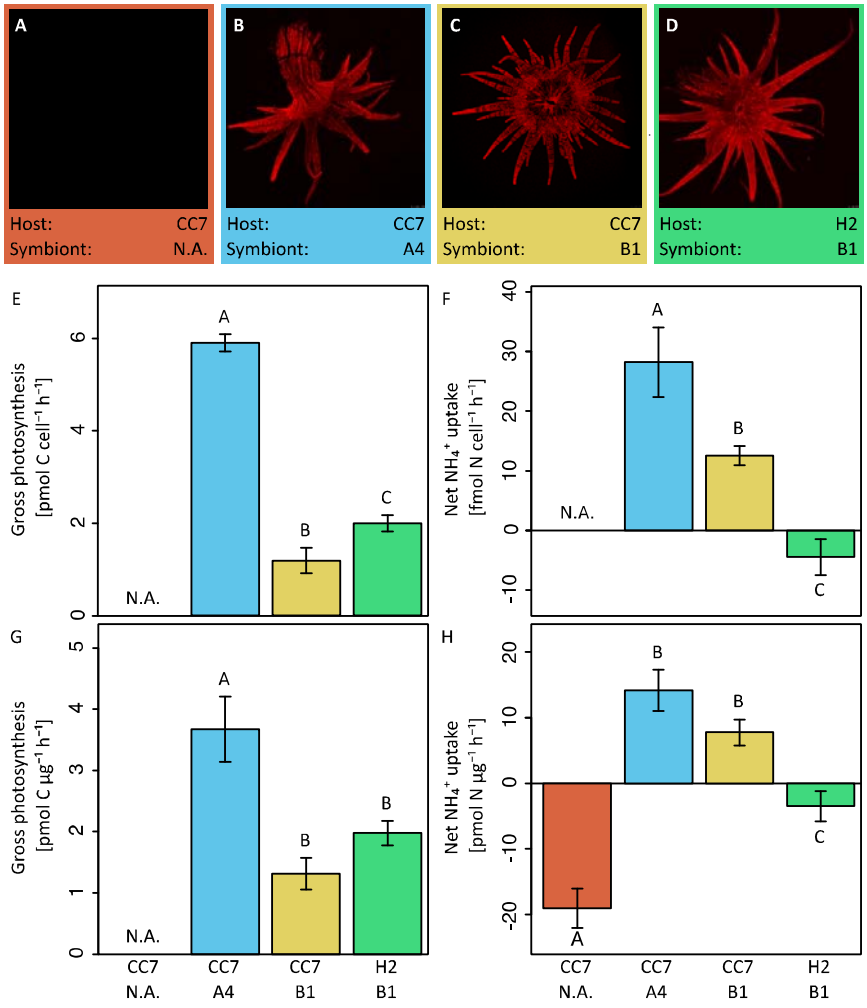

693

694 **Fig. 1** Ammonium (NH_4^+) uptake and carbon fixation (gross photosynthesis) of Aiptasia.

695 Fluorescence microscopy overview of the four host–symbiont combinations **(A-D)** to

696 visualizes chlorophyll autofluorescence of endosymbiotic *Symbiodinium*. Gross

697 photosynthesis **(E,G)** and net NH_4^+ uptake **(F,H)** of Aiptasia were normalized either to

698 symbiont density **(E,F)** or total host protein content **(G,H)**. Gross photosynthesis rates were

699 calculated as the sum of net photosynthesis and respiration rates ($P_G = P_N + R$). Net NH_4^+

700 uptake was quantified with the ammonium depletion method. All data shown as mean ± SE.

701 Different letters above bars indicate significant differences between groups ($p < 0.05$).

bioRxiv preprint first posted online Nov. 22, 2017; doi: http://dx.doi.org/10.1101/223933. The copyright holder for this preprint (which was not peer-reviewed) is the author/funder. It is made available under a CC-BY 4.0 International license.

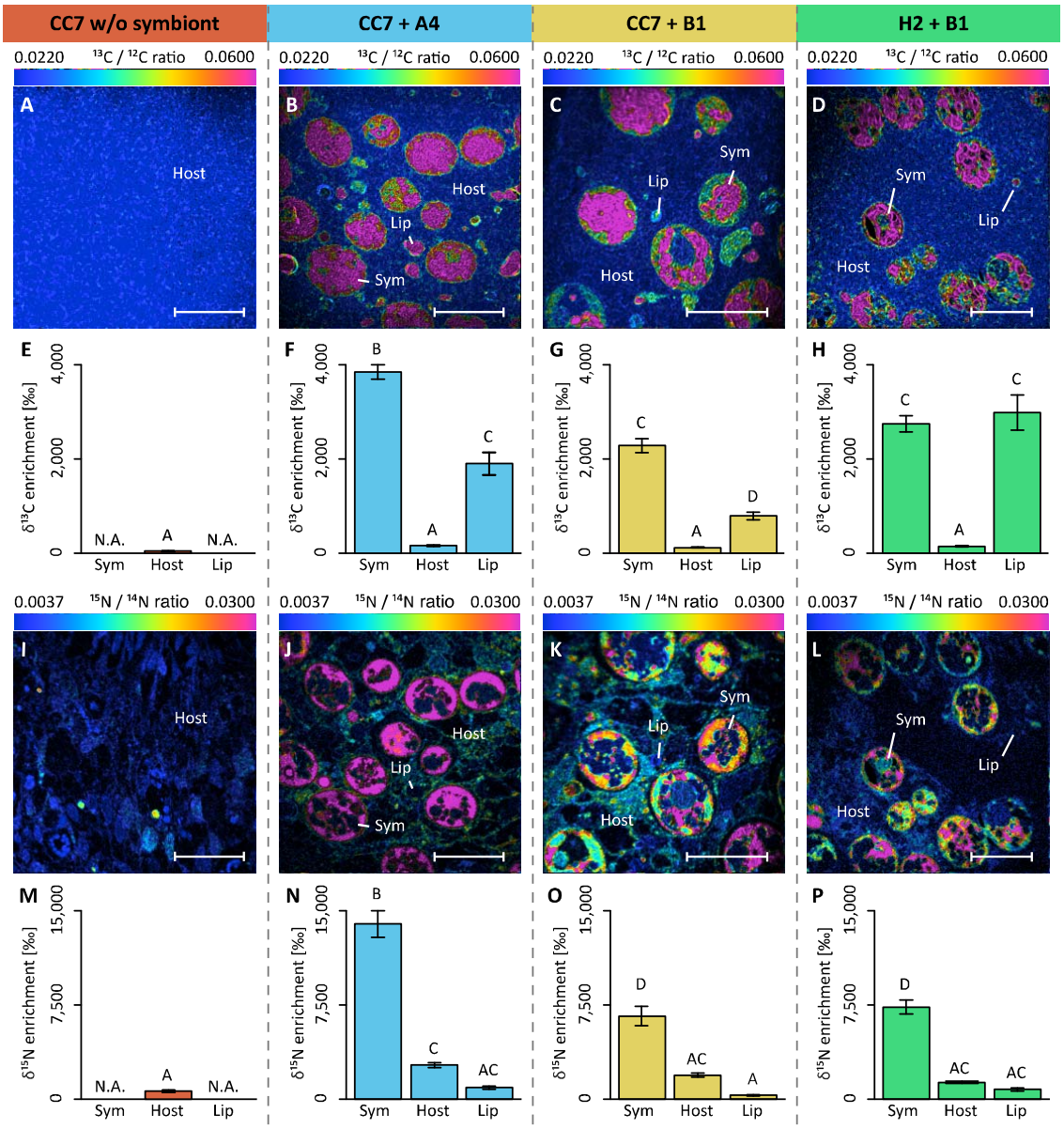

Fig. 2 NanoSIMS imaging and quantification of cell specific carbon (as ^{13}C-bicarbonate) and nitrogen (as ^{15}N-ammonium) assimilation within the Aiptasia—*Symbiodinium* symbiosis. Representative images of the distribution of $^{13}C/^{12}C$ ratio **(A-D)** and of $^{15}N/^{14}N$ ratio **(I-L)** within the Aiptasia holobiont are displayed as Hue Saturation Intensity (HSI). The rainbow scale indicates the $^{13}C/^{12}C$ and $^{15}N/^{14}N$ ratio, respectively. Blue colors indicate natural abundance isotope ratios shifting towards pink with increasing ^{13}C and ^{15}N incorporation levels, respectively. Corresponding δ^{13}C enrichment **(E-F)** and δ^{15}N enrichment **(M-P)** in the

bioRxiv preprint first posted online Nov. 22, 2017; doi: http://dx.doi.org/10.1101/223933. The copyright holder for this preprint (which was not peer-reviewed) is the author/funder. It is made available under a CC-BY 4.0 International license.

710 tissues of the four host–symbiont combinations. For each NanoSIMS image, the $\delta^{13}C$ (E-F)
711 and $\delta^{15}N$ (M-P) enrichment were quantified for individual Regions Of Interest (ROIs) that
712 were defined in OpenMIMS by drawing (I) the contours of the symbionts, and circles
713 covering (II) the adjacent host tissue and (III) the host lipid bodies. Scale bars represent 10
714 µm. Abbreviations: Sym = *Symbiodinium* cell, Host = tissue (host) & Lip = lipid body (host).
715 All data shown as mean ± SE. Different letters above bars indicate significant differences
716 between groups ($p < 0.05$).
717